Supplement: Retrieval of ultra-violet aerosol absorption from radiation measurements in young wildfire plumes

Correspondence: Jan-Lukas Tirpitz (jltirpitz@gmail.com) and Jochen Stutz (jochen@atmos.ucla.edu)

S1 Time series of individual retrievals for Lefthand and Williams Flats fires

Section 4.1 in the main text discusses the results of individual retrievals, but only shows data from the Shady fire (Figure 5 in the main text). This section provides similar figures for the Williams and the Lefthand fires (Figure S1 and Figure S2 respectively).

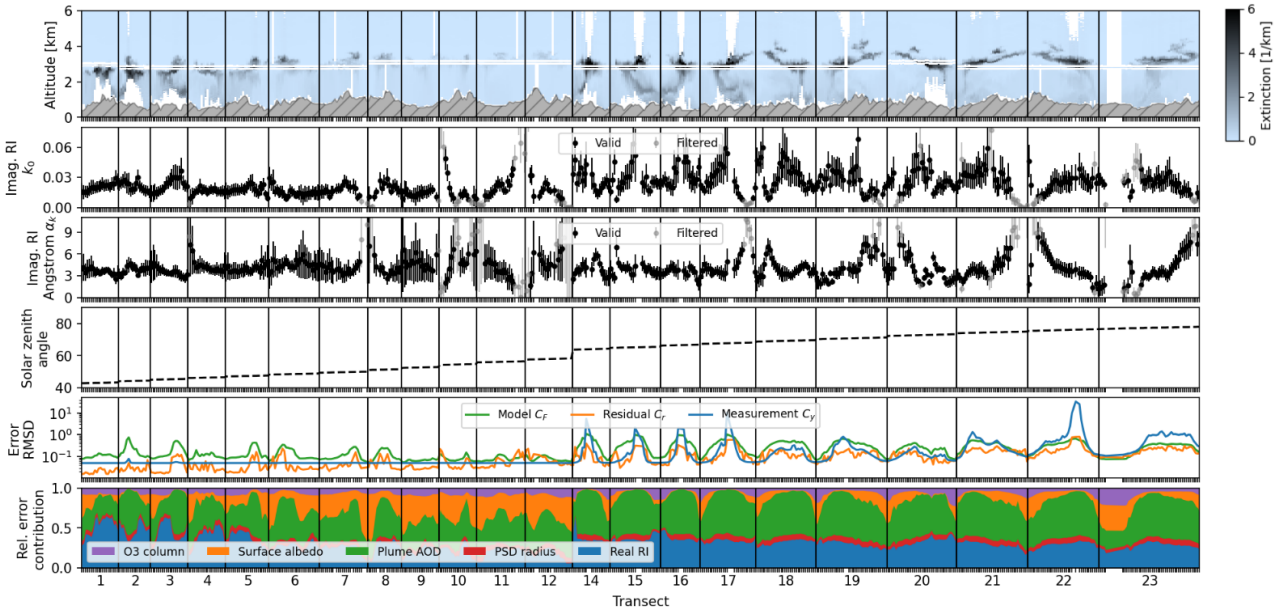

Figure S1. Results from retrievals performed on individual lidar profiles from transects of Williams Flats fire. Panel A shows the plume cross-sections as Lidar curtains of aerosol extinction coefficient. Panels B and C show the retrieval results of imaginary RI k_0 (at 387 nm) and angstrom coefficient α_k. Error bars indicate propagated uncertainties according to Eq. 11 in the main text. Grey data points are flagged as invalid according to the filter criteria described in Section 4.2 in the main text. Panel D shows solar zenith angle. Panel E indicates contributions of model error $\mathbf{C_F}$, fit residual $\mathbf{C_r}$ and measurement error $\mathbf{C_y}$ to the total retrieval uncertainty $\hat{\mathbf{C}}_\mathbf{x}$. Values represent RMSDs over the diagonal of the corresponding covariance matrix. Panel F illustrates the relative contributions of each critical fixed parameter to the total model covariance $\mathbf{C_F}$.

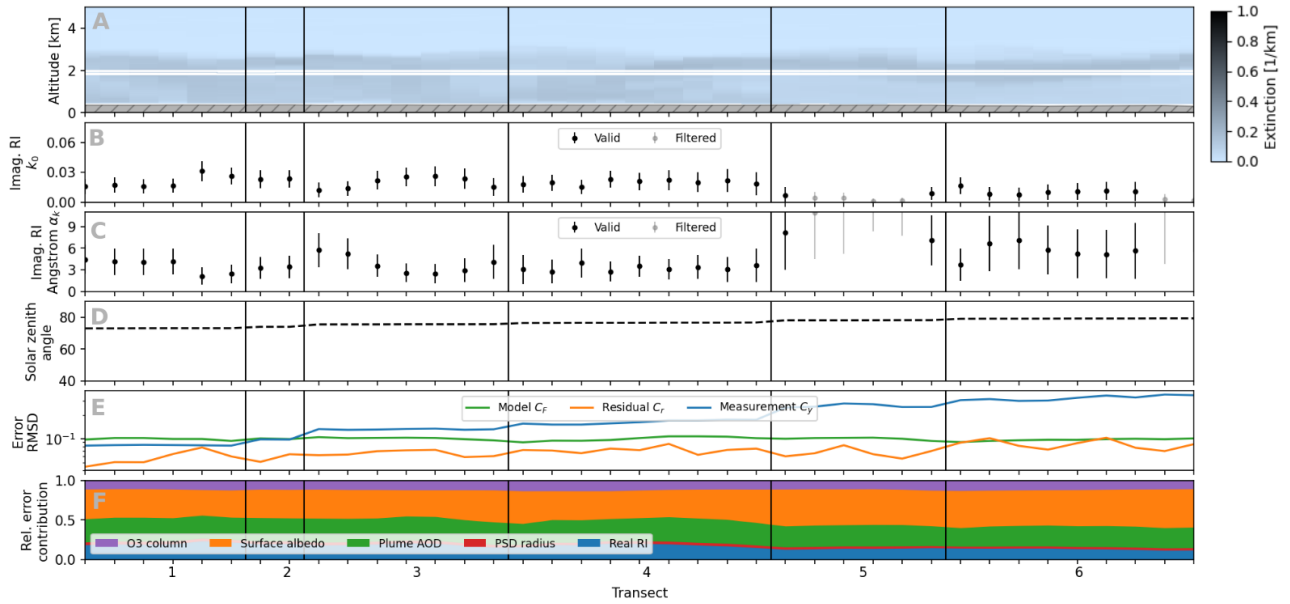

Figure S2. Results from retrievals performed for the Lefthand fire. See the Figure S1 caption for details.

S2 Determining the ideal retrieval conditions

The quality of the retrieval results depends on a number of factors (see Section 4.1 in main text for a detailed description). To determine the ideal retrieval conditions, we calculated errors of the retrieved parameters and the correlation between them for various synthetic scenarios reflecting typical conditions. The simulations assume a Gaussian-shaped BB plume with a vertical extent (full-width half-maximum) of 1 km and a center height of 2.5 km above the ground, which is at 2 km above sea-level (Figure S3). We used typical plume aerosol properties, based on FIREX-AQ measurements, literature values and retrieval results from this study. The SZA is assumed fixed to 30°. Uncertainties in the fixed critical model parameters are assumed to be 20 % on the PSD parameters, the real part of the refractive index, and the AOD and surface albedo, plus 5 % on the total ozone column.

We found that the most important factors controlling error levels are the flight altitude (with respect to the plume), and the plume AOD (Figure S3). Smallest retrieval errors and correlations were found when the aircraft is in the middle to upper part of the plume (Figure S3, A). In such cases the impact of dubious assumptions on the surrounding environment is minimized. For instance, the impact of surface properties or background aerosols on the radiation field becomes small compared to the plume aerosol signal. At the same time, downwelling and upwelling radiation provide mostly independent information (downwelling radiation is dominated by direct beam attenuation; upwelling radiation includes an additional in-plume scattering event), maximizing the information content in the measurements. In terms of AOD, best results are achieved for AODs of 3 to 5 at 532 nm (Figure S3, B). For lower values of AOD, the aerosol signal decreases, while for high AOD, there is insufficient

light reaching the instrument.

It should be noted that this analysis omits errors potentially arising from 3D radiative transfer effects. These can only be estimated using 3D RT models, which we considered to be out of the scope of the present study.

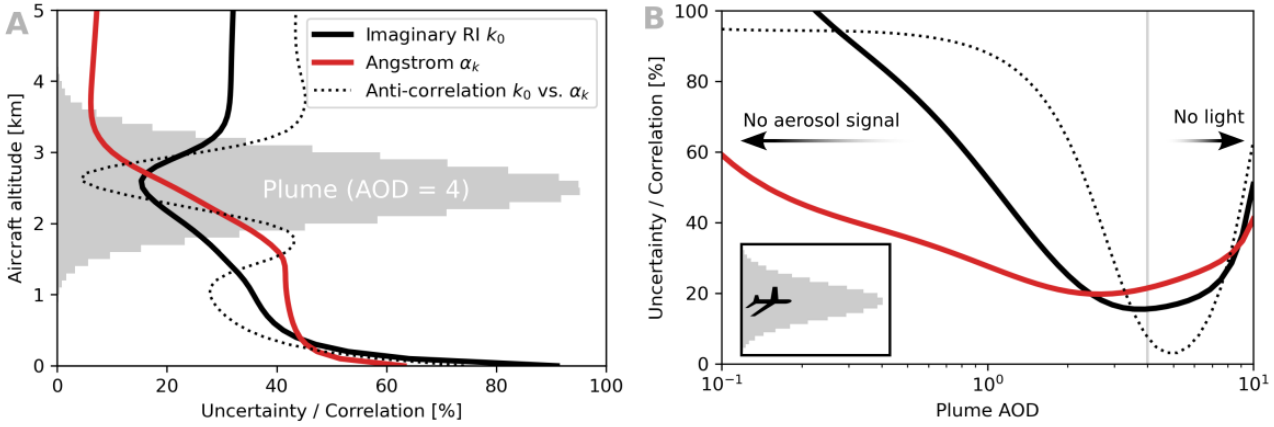

Figure S3. Errors and correlation for the retrieved parameters as functions of the flight altitude (panel A) and plume AOD (panel B). Simulations are based on synthetic scenarios with a Gaussian-shaped plume (see text). Panel B assumes the aircraft to be in the middle of the plume. All AODs are given for 532 nm.

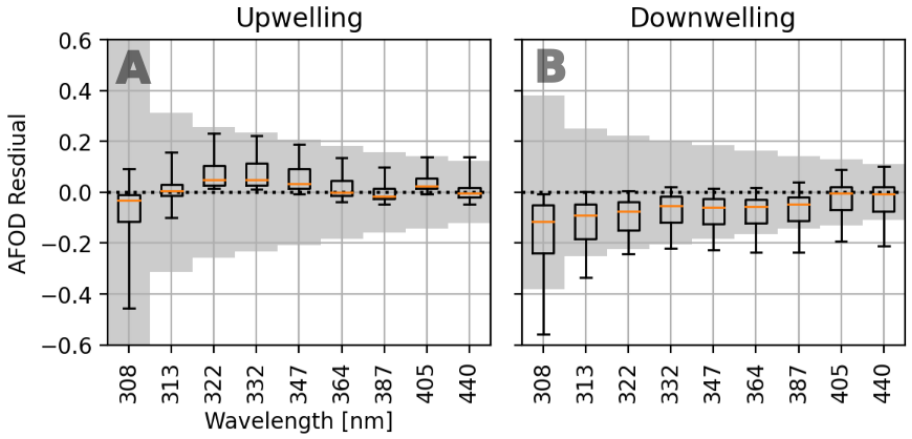

Figure S4. Statistics of the model-measurement residual in terms of AFOD (see main text Section 3.4). Orange lines indicate the median, boxes span the 25th to 75th percentile. Grey shaded areas indicate of model and measurement errors ($\mathbf{S_F} + \mathbf{S_y}$).

S3 Individual retrieval results and transect averaging process

Figure S5 illustrates the filtering and transect averaging process, providing a detailed view of retrieved imaginary RI, as well as derived VAC and SSA for two Shady fire transects. Transect 4 represents a particularly good case, with little variation among the individual retrievals (panel A). Transect 17 shows more retrieval instabilities and contains a number of individual retrieval results that were filtered out (dotted lines in panel C), as they did not satisfy the k_0/α_k criterion described in section 4.2 in the main text. Such instability is likely due to a 3D radiative effects, which are expected to appear more frequently here due to the high SZA (78°). Despite the different behavior of the individual retrievals, the resulting transect averages (panel B and D) agree well. Furthermore, the similar magnitudes of propagated uncertainties and scatter (RMSD) support the validity of our error propagation scheme.

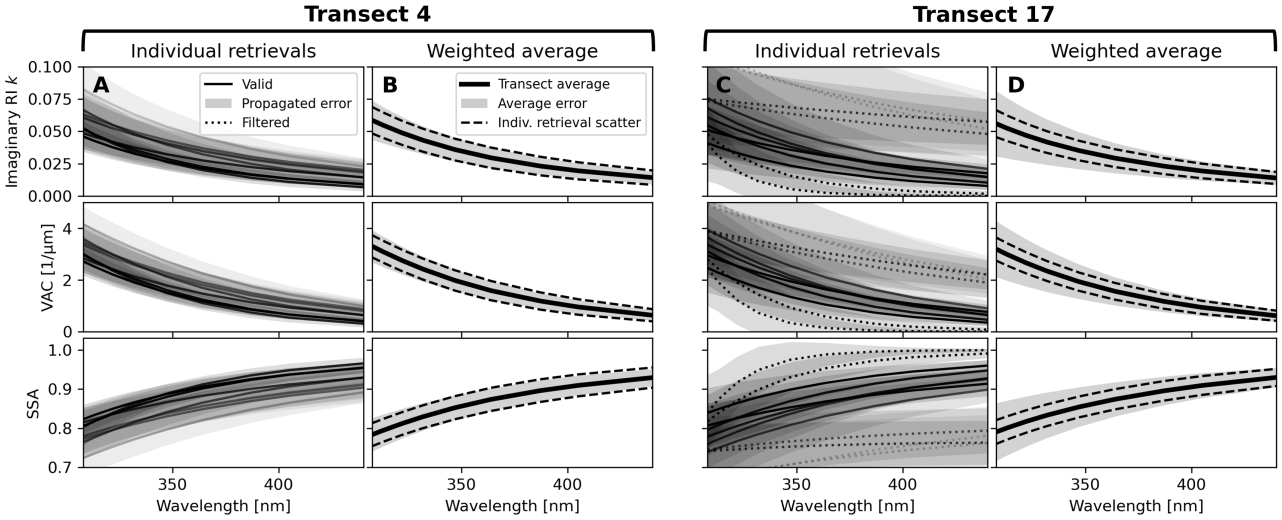

Figure S5. Spectrally resolved imaginary RI, volume absorption cross section (VAC), and single scattering albedo (SSA), for two transects from the Shady fire. Panel columns A and C show the results for the transect's individual retrievals. Transparency in the gray-shading indicates the level of uncertainty. Dotted lines indicate retrievals not satisfying the k_0/α_k filter criterion described in the main text. Panel columns B and D show error-weighted transect averages, where the dashed lines indicate the scatter (RMSD) between individual retrievals.

S4 Other complementary figures

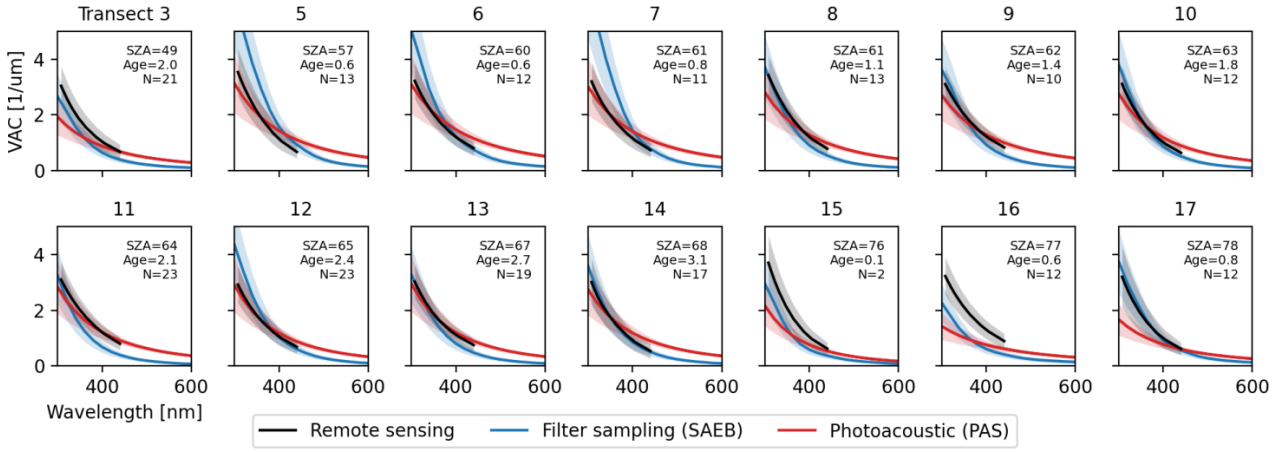

Figure S6. Adjunct to figure 7 in the main text. While Figure 7 summarizes the comparison between different measurement techniques in a statistical boxplot, this figure shows the data for each transect. Inserts list the SZA in degrees, the plume age in hours, and the number of individual retrievals contributing to the transect.

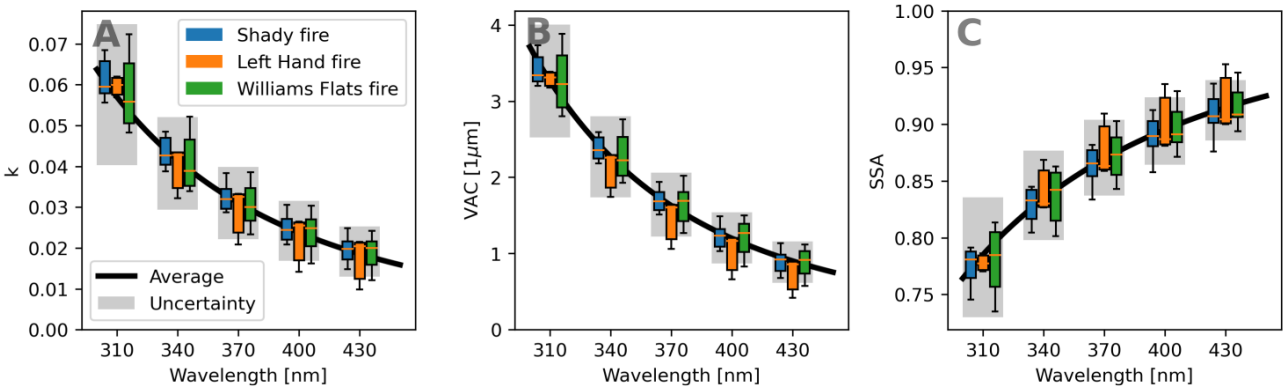

Figure S7. Same as Figure 9 in the main text but with relaxed settings for the filtering based on the k_0/α_k ratio, as described in Section 4.2. In Figure 9 we discarded retrieval results where k_0/α_k deviates from its median value by more than a factor of 5 or 0.2 in the upper or lower direction, respectively. Here, we allow for deviations by more than factors 10 and 0.1 respectively. The resulting increase in scatter and changes in the average results (compare figure 9) are negligible compared to the propagated uncertainties.

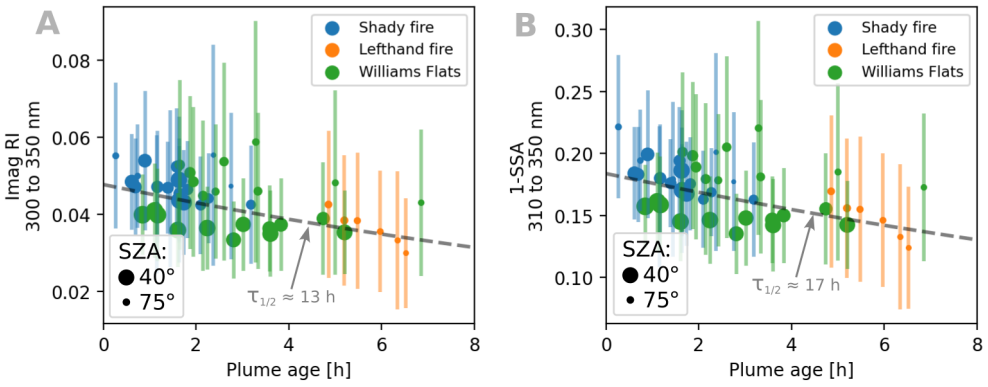

Figure S8. Dependence of imaginary RI (panel A) and 1-SSA (panel B) on plume age. Error bars represent propagated errors. Marker size indicates $\cos(\mathrm{SZA})$, as a proxy for the solar exposure. The grey dashed line shows an exponential fit, based on all data points.